The Principle of Natural Proportionality applied to the creep of compacted recycled asphalt pavement

Eulalio Juárez-Badillo
Graduate School of Engineering, National University of Mexico

2011 Pan-Am CGS Geotechnical Conference

ABSTRACT
General theoretical equations provided by the principle of natural proportionality are used to describe the creep response of compacted RAP under sustained deviatoric stresses. Constant stress, consolidated-drained triaxial tests were performed on 100 mm diameter, compacted RAP specimens at multiple confining stresses and deviator stress levels.

RESUMEN
Las ecuaciones generales previstas por el principio de proporcionalidad natural se usan para describir la respuesta de creep de RAP compactadas bajo esfuerzo desviador sostenido. Pruebas triaxiales de esfuerzo constante y consolidadas-drenadas fueron realizadas sobre muestras compactadas de RAP de 100 mm de diámetro, para múltiples esfuerzos de confinamiento y niveles de esfuerzo desviador.

1 INTRODUCTION

"Creep of compacted recycled asphalt pavement" is the title of a paper published by Viyanant C. et al. (2007) in the Canadian Geotechnical Journal. After reading this paper the author was interested in applying the theoretical equations provided by the Principle of Natural Proportionality to describe the experimental data contained in this paper. The result is the subject of this paper. The author suggests to the readers of this paper to read first the above reference for a complete information of the tests performed. Some information follows.

2 MATERIAL DESCRIPTION

"RAP is derived from demolished asphalt pavement and is generated by milling or full-depth removal of asphalt pavement. Milling involves the mechanical removal of up to 50 mm of pavement in a single pass. Full-depth removal is usually achieved with a pneumatic pavement breaker or a rhino horn on a bulldozer. The broken materials are transferred to a central facility for a series of recycling processes, which include crushing, screening, conveying, and stacking. Asphalt pavement can also be pulverized in place and incorporated into granular or stabilized base courses using a self-propelled pulverizing machine (FHWA. 2000), which eliminates the cost of transporting material to and from the processing facility. The processing practice generally yields RAP with a consistent gradation."

"The parent material for RAP is obviously the original asphalt pavement. Asphalt pavement is a blend of aggregate and bituminous asphalt cement binder, with typical mix proportions ranging from 3% to 7% asphalt cement (Roberts et al. 1996). The processed RAP material contains aggregate particles that are coated with asphalt cement, such that asphalt cement is found at most of the grain contacts. Thus, while the properties of RAP are affected by traditional geotechnical parameters such a in-place density, material gradation, and particle shape, the properties are also affected by the presence and character of the asphalt cement binder. The asphalt cement binder is a hydrocarbon derived from the distillation of crude oil, and its properties (e.g., viscosity, ductility) are controlled by the type of virgin crude oil and the distillation process (Roberts et al. 1996). AASHTO MP1a-04 (AASHTO, 2004) provides standard specifications for asphalt cement binders that are based on achieving specific properties at specific temperature, such that the appropriate asphalt cement performance grade can be selected for the range of temperatures expected in a region."

"For this study, a bulk sample of RAP was obtained from a Texas Department of Transportation stockpile within the Corpus Christi District. The asphalt cement content of the RAP was estimated using a nuclear gauge, which measures the hydrogen content of a material (ASTM method 4125-05) (ASTM 2005a). After correcting for the water content of RAP, the asphalt cement content was estimated as 3.5%. It was not possible to determine the type of asphalt cement used in the parent hot-mix asphalt for the RAP used in this study, but performance grades 70-22 and 76-22 are used most often in Texas."

"Figure 1 displays the grain size distribution of RAP samples taken from four different locations in the RAP stockpile. The grain size distribution of the RAP was very consistent in the stockpile. Less than 5% of the material was larger than 40 mm, and no particles larger than 75 mm were observed. Only 2% of the material passes the No. 40 sieve (0.425 mm), and there were no fines passing the No. 200 sieve (0.075 mm). The Unified Soil Classification System (USCS) classification of this material is well-graded gravel (GW). The gradation of the RAP across the stockpile was consistent with gradations generated by commercial procedures of RAP (Rathje et al. 2006) and generally meets gradation specifications for earth structures such as retaining walls."

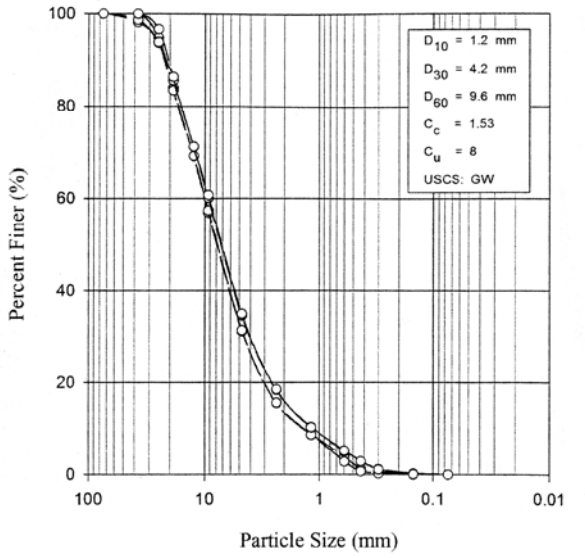

Figure 1. Gradation of RAP used in this study

3 EXPERIMENTAL PROGRAM

"Constant-stress, consolidated-drained triaxial creep tests were performed on 100 mm diameter compacted specimens of RAP. During testing the axial load was adjusted to maintain a constant axial stress as the cross-sectional area of the specimen changed. Drained tests were performed because a drained response is expected in the field due to the large hydraulic conductivity of RAP (k ~ 0.005 cm/s, Viyanant. 2006). The RAP sample was scalped at 16mm such that the maximum particle size of the RAP specimens was smaller than one sixth of the specimen diameter. Specimens were compacted at approximately 3% moisture content to a dry unit weight of 18.4 kN/m^3 resulting in a void ratio of 0.24. The specimens were tested at room temperature at effective confining pressures (σ'3) between 34 kPa (5 psi) and 340 kPa (50 psi), and at varying stress levels ( ). Each test lasted at least 1 week (~ 10,000 min) or until creep rupture occurred. A constant deviator stress was achieved throughout the 1 week testing period by increasing the axial load approximately to account for the increase in specimen diameter. Consolidated-drained, strain-controlled, monotonic triaxial tests were also performed at each confining stress to determine the deviator stress at failure for each confining pressure (Figure 2). These tests were performed at a strain rate of 0.5%/min until an axial strain of about 12%-14% was reached. At smaller confining pressures, the RAP displayed a slight peak in deviator stress that was accompanied by dilatant volumetric strain behavior. At larger confining pressures, the volumetric strain pressure was compressive and no peak was observed in the stress-strain curve. The secant friction angles, for these tests ranged from 54° at 34 kPa to 40° at 340 kPa, indicating a curved failure envelope over this range in confining pressure."

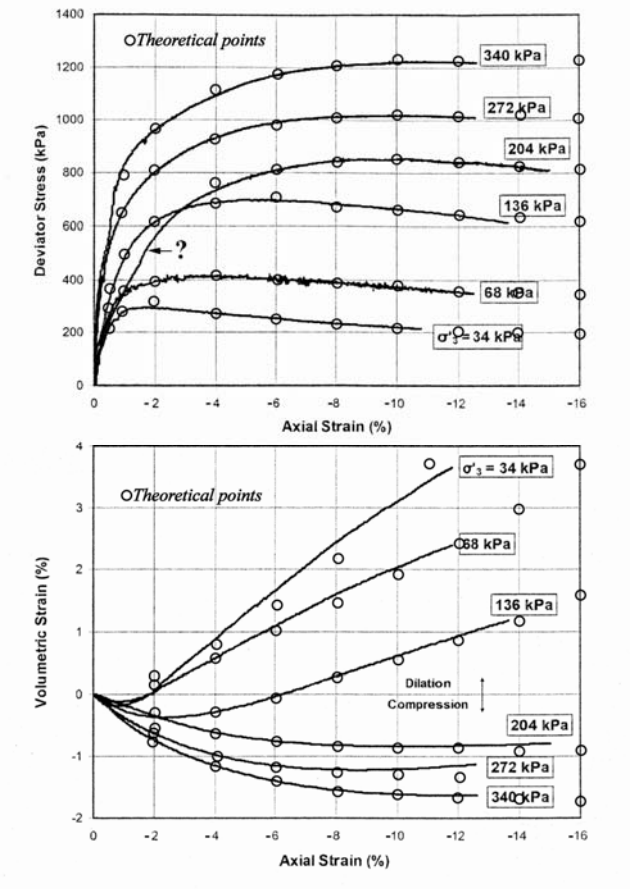

Figure 2. Results from consolidated-drained, monotonic triaxial tests on comptacted RAP

"Three series of creep tests were performed. The first test series was performed at an effective confining pressure of 136 kPa (20 psi), with ten specimens tested at stress levels ( ) between 0.40 and 0.88. The second test series included ten specimens tested at an effective confining pressure of 272 kPa (40 psi) and at stress levels between 0.50 and 0.90. The final test series included six specimens tested at stress levels of 0.8 and at confining pressures of 34, 68, 136, 204, 272, and 340 kPa (5, 10, 20, 30, 40, and 50 psi). Together these test series allow for an assessment of the creep-time response of RAP as a function of stress level and confining pressure, as well as an evaluation of the creep rupture response of RAP."

4 CREEP TIME RESPONSE

4.1 Test results at σ'_3 = 136 kPa

"Figure 3a is a plot of the measured axial creep strains (ε) versus log(time) for the ten tests performed at an effective confining pressure of 136 kPa. Tests with ≥ 0.64 reached the tertiary creep stage and creep rupture within 1 week after stress application. The creep tests performed at < 0.64 may have eventually reached creep rupture if the tests had continued, but based on the

axial strain rates observed at the end of 1 week, it would likely have taken more than a month for these specimens to reach complete creep rupture. At any given time, the magnitudes of the axial creep strains in Figure 3a are generally larger at the larger stress levels. The volumetric strains from these tests indicated compressive behavior during the primary and secondary stages of creep, but the specimens began to dilate as creep rupture was approached. Creep rupture will be discussed further in the next section of this paper."

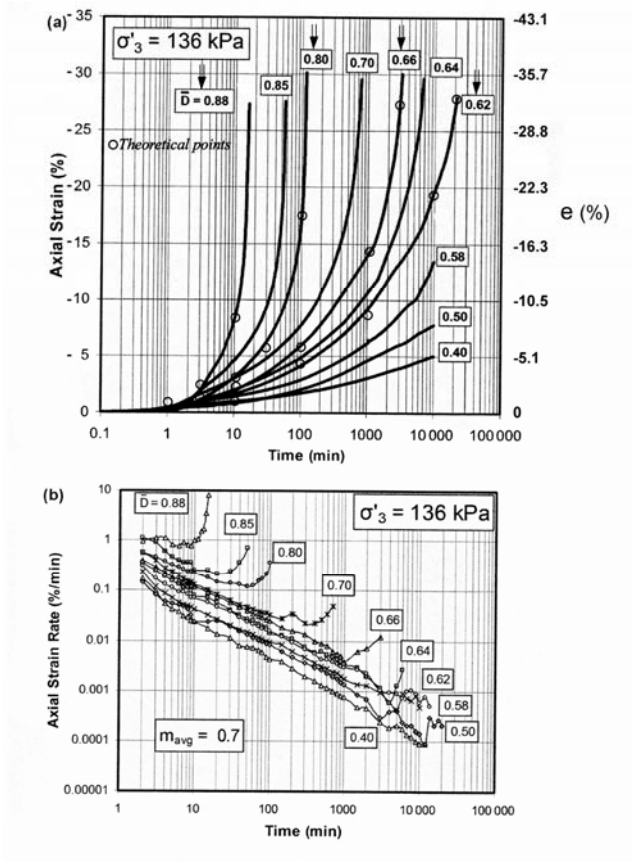

Figure 3. a) Axial strains and (b) axial strain rates measured in test on RAP specimens at σ'_3 = 136 kPa.

"The axial strain data in Figure 3a can be differentiated with respect to time to obtain the axial strain rate ($\dot{\varepsilon}$) as a function of time (Figure 3b). The initial strain rates are in the range of 0.1% / min to 1.0% / min and larger strain rates are observed for larger $\bar{D}$ values at any given time. The linear relationship between log($\dot{\varepsilon}$) and log(time) is clearly noticeable, particularly for $\bar{D} \leq 0.70$. At $\bar{D} \geq 0.64$, this linear behavior is followed by an increase in strain rate as creep rupture is approached."

4.2 Test results at constant stress level

"To further investigate the effect of confining pressure on the creep response of RAP, a series of tests was performed at a constant value of $\bar{D}$ = 0.8 at six confining pressures ranging from 34 to 340 kPa. A large value of $\bar{D}$ was chosen to ensure that most of the specimens experienced creep rupture within the 1 week testing period. The measured axial strains and axial strains rates are plotted in Figure 4. The creep behavior model (equation 1) predicts that tests performed at the same $\bar{D}$ but at different confining pressures will produce the same strain rate behavior. However, the data in Figure 4 reveal different curves for each confining stress level, indicating that confining pressure significantly affects the creep behavior of RAP. However, the effect of confining pressure is not systematic. The creep strains increase as confining pressure increases from 34 to 136 kPa, but then decrease at larger confining pressures up to 340 kPa. Also, the tests at 34 and 68 kPa initially experience small creep stains but quickly accelerate to creep rupture, while the tests at larger confining pressures initially experience larger creep strains but take more time to reach creep rupture."

5 THEORETICAL EQUATIONS

The general theoretical equations provided by the Principle of Natural Proportionality are as follows (Juárez-Badillo, 1999):

The pre-peak normal function Y_N with $\nu = 2$

$$(\sigma_1 - \sigma_3) = (\sigma_1 - \sigma_3)_f \left\{1 - \left[1 - \frac{3e_a \sigma_{co}}{\mu(\sigma_1 - \sigma_3)_f}\right]^{-1}\right\} \qquad [1]$$

where $(\sigma_1 - \sigma_3)$ = maximum principal stress difference, e_a = axial natural strain σ_{co} = initial consolidation pressure, $(\sigma_1 - \sigma_3)_f = (\sigma_1 - \sigma_3)$ at $e_a = \infty$ and μ = shear coefficient. The natural axial strain e_a is given by

$$e_a = \ln(1 + \varepsilon_a) - \frac{\varepsilon_v}{3} \qquad [2]$$

where ε_a is the common (Cauchy) axial strain and ε_v is the natural volumetric strain. Observe that in triaxial compression tests e_a and ε_a are negatives.

The post-peak ductility function Y_D:

$$(\sigma_1 - \sigma_3) = (\sigma_1 - \sigma_3)_\infty + \left[(\sigma_1 - \sigma_3)_1 - (\sigma_1 - \sigma_3)_\infty\right]\left(\frac{e_a}{e_{a1}}\right)^{\frac{-1}{\nu}} \qquad [3]$$

where $(\sigma_1 - \sigma_3)_\infty = (\sigma_1 - \sigma_3)$ at $e_a = \infty$, $[e_{a1},(\sigma_1-\sigma_3)_1]$ is a known point and ν = ductility coefficient.

The volume change equation:

$$\frac{V}{V_o} = \left[1 + \frac{\Delta\sigma_i}{\sigma_{co}} + \alpha\, y - \alpha_e \left(\frac{\sigma_{eo}}{\sigma_{co}} - 1\right) y_e\right]^{-\gamma} \qquad [4]$$

where V = volume, V_o = initial volume, $\Delta\sigma_i$ = isotropic stress increment, σ_{eo} = initial equivalent consolidation pressure due to interlocking of the solid particles, γ = natural coefficient of compressibility, y = sensitivity function given by:

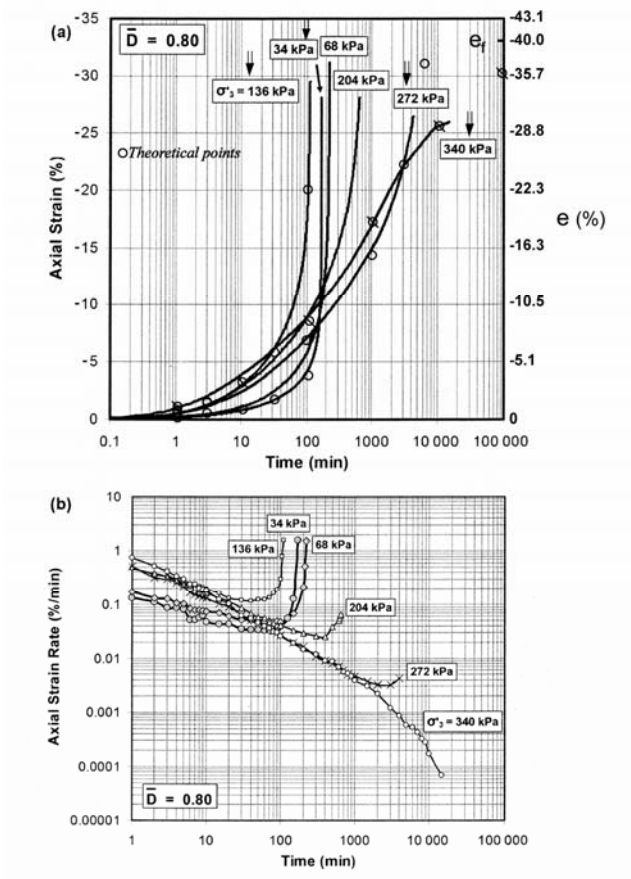

Figure 4. (a) Axial strains and (b) axial strain rates measured in test on RAP specimens at $\overline{D}$ =0.8 and varying σ_3.

$$y = \left[1 + \left(\frac{e_a}{e_a^*}\right)^{-\beta}\right]^{-1} \qquad [5]$$

where α and β = pore pressure coefficients, $e_a^* = e_a$ at y = 0.5. The subindex e in the third term of (4) is only to distinguish the values α and y of the third term with respect to the second term. Similarly in Equation [5] for y_e are used the symbols β_e and e_{ae}^* Figures. 5, 6 and 7 present graphs of Y_N[1], Y_D[3] and Y[5].

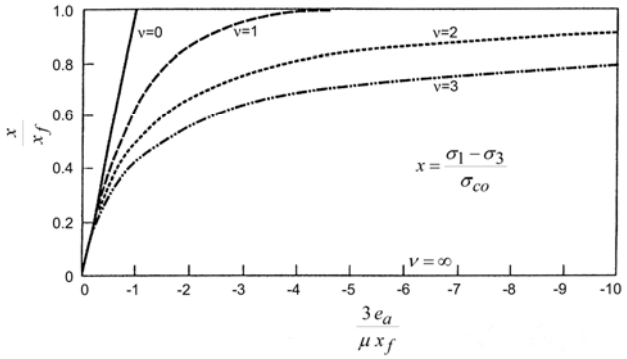

Figure 5. Prepeak normal function Y_N.

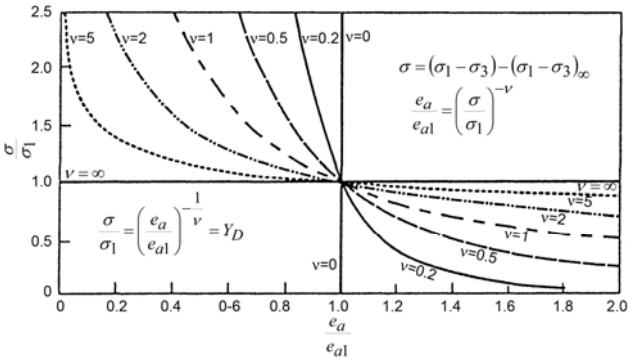

Figure 6. Postpeak ductility function Y_D.

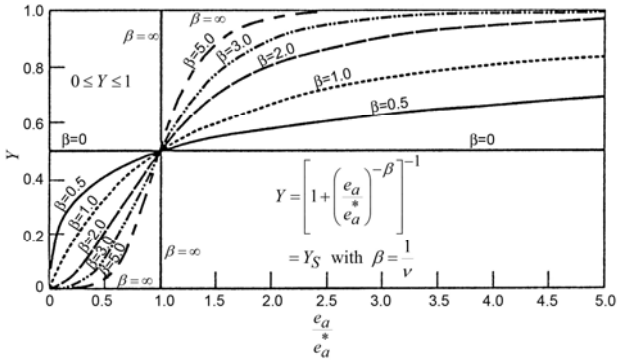

Figure 7. Sensitivity function Y.

The theoretical equations for creep read (Juárez-Badillo. 1994). For the stable zone:

$$e = \frac{e_f}{1+\left(\frac{t}{t^*}\right)^{-\xi}} \qquad [6]$$

where $e = e_a$, t = time, e_f = final e at $t = \infty$, $t^* = t$ at e = (1/2) e_f and ξ = natural fluidity coefficient.

For the unstable zone:

$$e = e^*\left(\frac{t_f}{t}-1\right)^{-\xi} \qquad [7]$$

where t_f = final t at $e = \infty$ and $e^* = e$ at t = (1/2) t_f. In the unstable zone the strain rate $\dot{e}$ is given by

$$\dot{e} = \xi\frac{e}{t}\left(1-\frac{t}{t_f}\right)^{-1} \qquad [8]$$

and we obtain:

$$\frac{d\dot{e}}{dt} = 0 \text{ at } t = t' = \frac{1-\xi}{2}t_f \qquad [9]$$

and at $t = t'$

$$\left(\dot{e}\right)_{\min} = 4\frac{\xi}{1-\xi^2}\frac{e}{t_f} \qquad [10]$$

6 PRACTICAL APPLICATION

The theoretical Equations [1] to [5] were applied to Figure 2. Table 1 shows the parameter values for this figure and the theoretical points are marked on it. It should be observed that the axial strains contain the isotropic strains of the volumetric strains. The author did not make the corrections indicated by [2] mainly because he had some difficulty in getting good experimental data for the pre-peak at low confining stresses. See for example the interrogation mark for σ'_3 = 204 kPa where the experimental data crosses the experimental curves of other tests. This is reflected, I believe, in some different values for β_e at low confining stresses. Observe, however, that all tests showed a natural coefficient of compressibility γ = 0.019 and all showed also $\alpha_e = \alpha = 1$ and $\beta = 2$. The interlocking of solid particles decreased from a value of σ_{e0}/σ_{c0} =11.8 for σ'_3 = 34 kPa to a value σ_{e0}/σ_{c0} = 1.6 for σ'_3 = 340 kPa. A value of $\sigma_{e0}/\sigma_{c0} = 1$ indicates no interlocking of solid particles.

Another important observation is that $(\sigma_1 - \sigma_3)_\infty = 3.5294\sigma'_3$ for all values of σ'_3, from 34 kPa to 340 kPa. For simplicity the volumetric strain in [4] was calculated with $\Delta\sigma_i$ obtained from the pre-peak theoretical equation; this is reflected with some small differences among experimental and theoretical points in small values of σ'_3, say σ'_3 = 34 and 68 kPa where the post-peak values of stresses are somewhat smaller than those given by pre-peak equations.

The theoretical creep Equations [6] and [7] were applied to Figures 3 and 4, only to the tests marked with an arrow; the parameter values appear in Table 2. Observe that only in Figure 4, $\overline{D}$ = 0.80 and $\sigma'3$ = 340 kPa the creep was in the stable zone, all other were in the unstable zone. The natural fluidity coefficient ξ varied between 1/3 and 2/3 with some values of 1/2.

7 CONCLUSIONS

The main conclusions are that the recycled asphalt pavement showed in these tests a value of the natural coefficient of fluidity ξ between 1/3 and 2/3 with various values of 1/2 and a natural coefficient of compressibility γ =0.019.

Table 1. Parameter values for Figure 2.

σ'_3 kPa	Pre-peak $Y_N(\nu=2)$		Post-peak, $Y_D(\nu=3)$			Volumetric strain							
	$(\sigma_1-\sigma_3)_f$ kPa	μ	ε_{a1}	$(\sigma_1-\sigma_3)_1$ kPa	$(\sigma_1-\sigma_3)_\infty$ kPa	α	β	e^*_a	α_e	β_e	e^*_{ae}	$\frac{\sigma_{eo}}{\sigma_{co}}$	γ
34	380	0.001	-0.12	205	120	1	2	-0.001	1	0.25	-0.100	11.8	0.019
68	440	0.001	-0.12	355	240	1	2	-0.005	1	0.25	-0.100	8.5	0.019
136	790	0.003	-0.12	640	480	1	2	-0.020	1	0.50	-0.100	7.1	0.019
204	910	0.005	-0.12	840	720	1	2	-0.025	1	2.0	-0.015	2.8	0.019
272	1,080	0.005	-0.12	1,020	960	1	2	-0.025	1	2.0	-0.009	2.2	0.019
340	1,300	0.005	-0.12	1,225	1,200	1	2	-0.060	1	2.0	-0.001	1.6	0.019

Table 2. Parameter values for Figures 3 (σ'_3=136 kPa) and 4 ($\overline{D}$ =0.80).

$\overline{D}$	t_f min	e^*, %	ξ	σ'_3 kPa	t_f min	e^* %	ξ	e_f %	t^* min	ξ
0.88	17	-7.0	0.660	34	180	-3.5	0.5	-	-	-
0.80	130	-10.5	0.500	136	120	-10.0	0.5	-	-	-
0.66	5,000	-27.0	0.400	272	7,200	-28.0	0.333	-	-	-
0.62	32,000	-28.0	0.333	340	-	-	-	-40	1,200	0.5

8 ACKNOWLEDGMENTS

The author is very grateful to Mrs. Juliana Constanza Zapata-Chica and to Mr. Sergio Hernández-Mira for their assistance in the preparation of this paper.

9 REFERENCES

Juárez–Badillo, E. (1994). "General stress-strain-time equations for soils", *XIII Int. Conf. on Soil Mech. and Found. Engng.* New Delhi, India, (1): 337-348.

Juárez–Badillo, E. (1999). "Static liquefaction of very loose sands: Discussion", *Canadian Geotechnical Journal* 36(5): 967-973.

Viyanant Chirayus, Rathje Ellen M., and Rauch Alan F. (2007). "Creep of compacted recycled asphalt pavement", *Canadian Geotechnical Journal* 44(6): 687-697.